Reflection of waves from slowly decaying complex permittivity profiles

S. A. R. Horsley,[1,*] M. Artoni,[2,3] and G. C. La Rocca[4]
[1]*Department of Physics and Astronomy, University of Exeter, Stocker Road, Exeter, EX4 4QL, United Kingdom*
[2]*European Laboratory for Nonlinear Spectroscopy, I-50019 Sesto Fiorentino, Italy*
[3]*Department of Engineering and Information Technology CNR-IDASC Sensor Lab, Brescia University, I-25121 Brescia, Italy*
[4]*Scuola Normale Superiore and CNISM, I-56126 Pisa, Italy*
(Received 10 June 2016; published 2 December 2016)

Wave propagation through rapidly but continuously varying media is surprisingly subtle, and in a pair of recent papers [Horsley *et al.*, J. Opt. **18**, 044016 (2016); Longhi, Eur. Phys. Lett. **112**, 64001 (2015)] it was found that planar media with a spatially varying permittivity $\epsilon(x)$ obeying the spatial Kramers-Kronig relations do not reflect waves incident from one side, however rapid the changes in $\epsilon(x)$. Within this large class of media there are some examples where the dissipation or gain is not asymptotically negligible and it has been pointed out [Longhi, Eur. Phys. Lett. **112**, 64001 (2015)] that it is impossible to define meaningful reflection and transmission coefficients in such cases. Here we show—using an exactly soluble example—that despite the lack of any meaningful reflection and transmission coefficients, these profiles are still reflectionless from one side in the sense that the profile generates no counterpropagating wave for incidence from one side. This finding is demonstrated through examining the propagation of pulses through the profile, where from one side we find that no second reflected pulse is generated, while from the other there is. We conclude with a discussion of the effect of truncating these infinitely extended profiles, illustrating how the reflectionless behavior may be retained over a wide range of incident angles.

DOI: 10.1103/PhysRevA.94.063810

I. INTRODUCTION

A rapid change in the speed of a wave usually results in some reflection, a phenomenon that is well understood for very abrupt changes. For instance, the reflection of electromagnetic waves from an interface between two dielectric media is governed by Fresnel's equations [1], which have long been used to design many things, from antireflection coatings to interferometers. Although there may be specific angles, such as Brewster's angle, where the reflection from a planar medium vanishes, it is typically nonzero. Meanwhile, a rapid but continuous change of material properties can act on an incident wave in a counterintuitive way ([2]). For example, a transformation medium [3] can exhibit arbitrarily large variations of refractive index over arbitrarily small distances, while remaining reflectionless for all incident fields. It is also known that the Pöschl-Teller profile $\epsilon(x) = 1 + 2[k_0 a \cosh(x/a)]^{-2}$ is reflectionless for all incident fields of frequency $\omega = ck_0$ [4–6], a property that has a deep connection with the solitons of the nonlinear Korteweg–de Vries equation [7], and the inverse scattering transform [8].

In recent work [9–11] it was found that there exists a very large class of continuously varying complex valued planar profiles that are reflectionless from one side, for all (or at least a wide range of) angles of incidence, despite exhibiting an arbitrarily rapid spatial variation. These inhomogeneous media are reflectionless for waves incident from, e.g., the left because the Fourier transform of the spatially varying permittivity $\epsilon(x) \to \tilde{\epsilon}(k)$ vanishes for $k < 0$. By analogy with the well-known frequency domain Kramers-Kronig relations [12], satisfied by virtue of a one-sided response in the time domain, these profiles satisfy the Kramers-Kronig relations with respect to the spatial coordinate x. This result extends previous work on complex valued periodic media found to exhibit "lop-sided" diffraction [13], or to be without stop bands at the Brillouin zone boundary [14]. We note that a special class of these profiles exhibit PT symmetry, which is known to suppress reflection [15]. We also note a related recent work by Philbin [16] that explores the possibility of eliminating reflection over all frequencies, for a fixed angle of incidence.

Typically, profiles satisfying the spatial Kramers-Kronig relations exhibit an electromagnetic response that decays to the background value (e.g., vacuum $\epsilon = 1$) as a power law rather than say an exponential, and there are subtleties about scattering from potentials that decay slowly to zero. Longhi has examined the additional conditions one must place on these profiles such that the scattering states are properly defined [11], finding that the integrated dissipation $I_\pm$,

$$I_\pm = \lim_{x \to \pm\infty} \int_0^x \mathrm{Im}[\epsilon(x')] dx', \tag{1}$$

must tend to a finite value. Waves propagating in profiles where (1) is not finite continually grow or diminish as $|x| \to \infty$ and it becomes impossible to define meaningful reflection or transmission coefficients. The main purpose of this paper is to assess whether profiles that do not satisfy (1) can in any sense be considered reflectionless from one side, despite the ambiguity in defining reflection and transmission coefficients. Through considering an exactly soluble example we shall show how the two counterpropagating waves can be identified within the contour integral representation of the solution. In addition we shall show that reflection can be identified as rapid spatial oscillations in the Poynting vector. To further establish the meaning of reflection in such profiles we numerically investigate the propagation of pulses emitted from a source embedded in the profile, finding that no reflected

*s.horsley@exeter.ac.uk

pulse is generated when the source is placed on one side. Finally we examine the effect of truncating these profiles to a finite width L, where in many cases the reflectionless behavior can be largely retained and it again becomes possible to define unambiguous values for the reflection and transmission coefficients.

II. PROPAGATION OF MONOCHROMATIC WAVES THROUGH A SLOWLY DECAYING PROFILE

To keep the discussion as simple as possible, we consider a particular permittivity profile (nonmagnetic, $\mu = 1$) that illustrates the nonreflecting behavior predicted in [9], but can be treated exactly in the monochromatic limit. This profile is defined in $x \in (-\infty, \infty)$ as

$$\epsilon(x) = 1 - \frac{A}{x + i x_0}, \tag{2}$$

with x_0 real and strictly positive [so that $\epsilon(z)$ is analytic in the upper half position plane]. This profile has already been discussed in [9] for real and positive values of A (making it purely lossy). It is interesting to study its behavior also for *complex* values of A as the profile still satisfies the Kramers-Kronig relations in space in this case, and thus ought to be nonreflecting for waves incident from the left. Recently, however, subtle issues have been raised [11] related to a proper definition of the scattering problem when the imaginary part of the profile decays to zero very slowly. In particular, when the imaginary part of A in (2) is *not* vanishing, the imaginary part of the profile goes asymptotically to zero as $-\mathrm{Im}[A]/x$, which means that the wave either asymptotically grows or diminishes as $|x| \to \infty$. Note also that for purely imaginary values of A the profile above is PT symmetric around $x = 0$ and has balanced loss and gain.

We demonstrate how the reflectionless behavior of the profile in (2) can be assessed even for complex values of A, generalizing the preliminary account presented in the supplementary information of [9]. The propagation of a monochromatic TE wave written as

$$\boldsymbol{E} = E_z(x)\, e^{i(k_y y - \omega t)}\, \hat{\boldsymbol{z}}, \tag{3}$$

where k_y is real, with $|k_y| < k_0 \equiv \omega/c$, is described by the Helmholtz equation which in this case takes the form,

$$\left[\frac{d^2}{dx^2} + k_0^2\left(1 - \frac{A}{x + i x_0}\right) - k_y^2\right] E_z(x) = 0. \tag{4}$$

The solutions to Eq. (4) can be written in terms of Whittaker functions (see formula 13.14.1 of [17]). But rather than appeal to properties listed in a mathematical table, here we directly examine the contour integral solution of (4), where the reflection and transmission of the waves can be clearly identified. To do this we write both solutions to (4) E_{z1} and E_{z2} as a right traveling wave times an envelope,

$$E_{zn}(x) = \exp(ikx) w_n(x), \tag{5}$$

(where $n = 1,2$) finding that the envelope obeys the differential equation,

$$z w_n''(z) + z w_n'(z) + \kappa w_n(z) = 0, \tag{6}$$

where $z = 2ik(x + i x_0)$, $k = (k_0^2 - k_y^2)^{1/2} > 0$, and $\kappa = i A k_0^2/2k$. Representing w as a contour integral,

$$w_n(z) = \int_{C_n} v(t) e^{tz} dt, \tag{7}$$

where n labels the chosen contours, which pick out different linear combinations of the two solutions to Eq. (6). Inserting this into (6), we find after an integration by parts that

$$\int_{C_n} \left[t(t+1)\frac{dv(t)}{dt} - (2t + 1 + \kappa) v(t)\right] e^{tz} dt = 0,$$

provided that

$$[t(t+1) v(t) e^{tz}]_{C_n} = 0,$$

where the subscript "C_n" indicates the difference in the bracketed quantity at the ends of this contour. The first of these two conditions can be satisfied if the integrand is zero, implying that the unknown function v must be given by

$$v(t) = \frac{v_0 t^{\kappa - 1}}{(1 + t)^{\kappa + 1}}, \tag{8}$$

where v_0 is an arbitrary constant which we set to unity in the remainder of this work. Having determined the quantity v to be given by (8), we have found the general solution to the Helmholtz Eq. (4), with different choices of the two contours C_1 and C_2 in (7) picking out different boundary conditions on the waves at infinity.

For large z the dominant contribution to the integral (7) comes from the vicinity of the points where the phase of the integrand is stationary, which we find to be

$$t_\pm = -\frac{1}{2} + \frac{1}{z} \pm \frac{1}{2}\sqrt{1 + \frac{4}{z^2} - \frac{4\kappa}{z}}. \tag{9}$$

To leading order the two points $t_\pm$ approach the branch points as z becomes large, as $t_- \sim -1 + (1 + \kappa)/z$ and $t_+ \sim (1 - \kappa)/z$. As we shall see, for large z these two points have a simple physical interpretation: *they, respectively, represent the left and right going waves within the profile*. The reflection from the profile can therefore be analyzed in terms of the relative contribution of the two points $t_\pm$ to the value of $w(z)$, as $x \to \pm\infty$.

Let us now examine the behavior of (7) in detail, assessing the relative combinations of left- and right-going waves, for the cases when waves are either incident from the left or the right of the profile. For waves incident from the left, we must pick the contour C such that on the far right of the profile, the contribution from the point $t = t_+$ dominates the integral. One such contour is C_1 illustrated in Fig. 1(b), and loops around the right-hand branch point of the function $v(t)$, beginning and ending on different Riemann sheets of this function. Meanwhile when waves are incident from the right, the point $t = t_-$ must dominate the integral on the far left of the profile. This is achieved with the contour C_2 illustrated in Fig. 1(a), looping around the left-hand branch point. Having drawn these two contours, and noting that increasing x leads to a counterclockwise rotation of their end points (the sense of rotation being determined by the sign of x_0) we can immediately see from Fig. 1 that the profile will reflect from only one side, independent of the angle of incidence

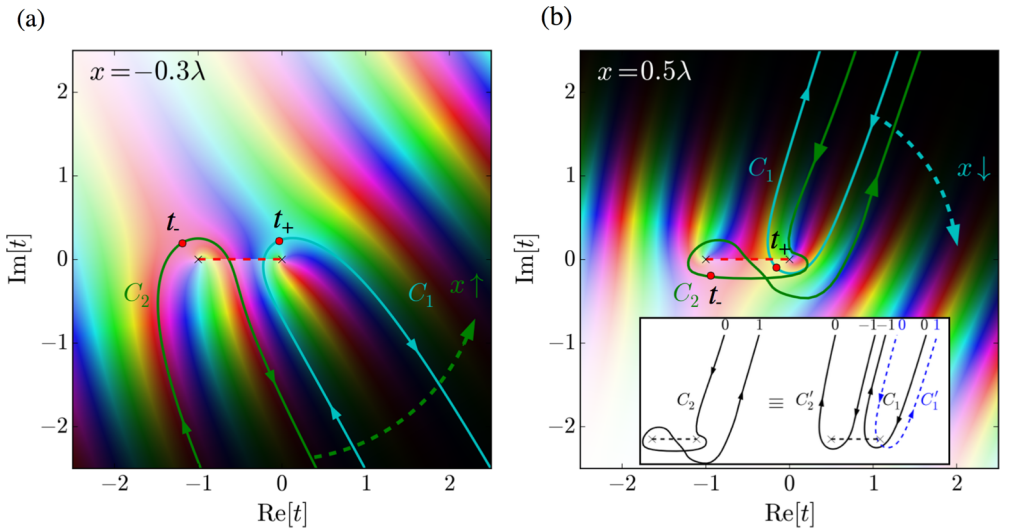

FIG. 1. Behavior of the integrand of $w(z)$ [see (7)] as a function of the dimensionless variable t. The brightness is proportional to the magnitude of the function, and the color indicates phase (advancing from zero to π in the succession, red, yellow, green, and light blue). The integrand has a branch cut between the points $t=0$ and $t=-1$, shown as a red dashed line, and points of stationary phase $t=t_\pm$ (9) are indicated by red dots. The dashed arrows in (a) and (b) show the motion of the end points of the contours C_1 and C_2 as the position x is increased or decreased, respectively. Comparing (a) and (b) we see that as x is increased (units $\lambda=2\pi/k_0$) from negative to positive, the end points of the two contours move counterclockwise from the lower to upper half of the t plane. This leaves the contour C_1 (waves incident from the left) still passing through t_+ only, while C_2 (waves incident from the right) becomes tangled around the branch cut, leading to contributions from both t_- and t_+ (inset showing how this tangled contour can be deformed into the succession of contours C_1, C_2', and C_1', with the numbers at the top indicating the Riemann sheet). When $x_0<0$, the sense of rotation of the contours is reversed.

$\cos(\theta)=k/k_0$, in accordance with the predictions of [9]. As C_1 is rotated counterclockwise it always passes through only one of the points of stationary phase t_+ because it loops around the right-hand branch point. Meanwhile because C_2 loops around the left-hand branch point, when it is rotated counterclockwise it ultimately becomes tangled around the branch cut, leading to contributions from both t_- and t_+, and hence reflection.

Evaluating the integral in the respective cases of contour C_1 (incidence from the left) at large positive x [see Fig. 1(b)] and contour C_2 (incidence from the right) at large negative x [see Fig. 1(a)] we obtain the respective forms of the waves on the transmission side of the profile,

$$w_1(z)=\int_{C_1}\frac{t^{\kappa-1}e^{tz}}{(1+t)^{\kappa+1}}dt \sim -2i\sin(\pi\kappa)\Gamma(\kappa)|z|^{-\kappa}e^{-ii\pi\kappa/2} \quad x\to+\infty, \tag{10}$$

and

$$w_2(z)=\int_{C_2}\frac{t^{\kappa-1}e^{tz}}{(1+t)^{\kappa+1}}dt \sim -2i\sin(\pi\kappa)\Gamma(-\kappa)|z|^{\kappa}e^{-z}e^{i\pi\kappa/2} \quad x\to-\infty, \tag{11}$$

where we have taken leading order terms in $1/z$, and applied the integral representation of the gamma function ([18], Sec. 8.31):

$$\Gamma(\kappa)=\frac{e^{-i\pi\kappa}}{2i\sin(\pi\kappa)}\int_{C'}e^{-t}t^{\kappa-1}dt, \tag{12}$$

with C' beginning at $+\infty+i0$ and ending at $+\infty-i0$, looping counterclockwise around the origin. Carrying out the same procedure in the opposite limits, of C_1 at large negative x [Fig. 1(a)] and C_2 at large positive x [Fig. 1(b)] we obtain the form of the waves on the side of the profile onto which the waves are incident,

$$w_1(z)\sim -2i\sin(\pi\kappa)\Gamma(\kappa)|z|^{-\kappa}e^{-3i\pi\kappa/2} \quad x\to-\infty, \tag{13}$$

and

$$w_2(z)=\left(\int_{C_1}+\int_{C_2'}+\int_{C_1'}\right)\frac{t^{\kappa-1}e^{tz}}{(1+t)^{\kappa+1}}dt \sim -2i\sin(\pi\kappa)\Gamma(-\kappa)e^{-i\pi\kappa/2} \times\left[|z|^{\kappa}e^{-z}-\frac{2\pi i e^{i\pi\kappa}}{\Gamma(1-\kappa)\Gamma(-\kappa)}|z|^{-\kappa}\right] \quad x\to+\infty, \tag{14}$$

where the integral over the tangled contour C_2 was evaluated through reducing it to the succession of three contours C_1, C_2', and C_1' shown in the inset of Fig. 1(b). To obtain (14) we also applied the identity $\Gamma(\kappa)\Gamma(1-\kappa)=\pi/\sin(\pi\kappa)$.

We have now completely determined the asymptotic behavior of waves incident from both left- and right-hand sides of the profile (2). Inserting (10–14) into the expression for the electric field (5) we have to leading order in $1/|z|$, for incidence from the left,

$$E_{z1}(x)=e^{ikx-\frac{iAk_0^2}{2k}\log(2k|x+ix_0|)} \times\begin{cases}1 & x\to-\infty\\ e^{-\frac{A\pi k_0^2}{2k}} & x\to+\infty\end{cases}, \tag{15}$$

and for incidence from the right,

$$E_{z2}(x) = \begin{cases} e^{-ikx} e^{\frac{iAk_0^2}{2k}\log(2k|x+ix_0|)} e^{-\frac{\pi Ak_0^2}{2k}} & x \to -\infty \\ e^{-ikx} e^{\frac{iAk_0^2}{2k}\log(2k|x+ix_0|)} + r\, e^{ikx} e^{-\frac{iAk_0^2}{2k}\log(2k|x+ix_0|)} & x \to +\infty, \end{cases} \tag{16}$$

where

$$r = |r|e^{i\phi} = -\frac{2\pi i e^{-2kx_0} e^{-\frac{\pi Ak_0^2}{2k}}}{\Gamma\left(1-\frac{iAk_0^2}{2k}\right)\Gamma\left(-\frac{iAk_0^2}{2k}\right)}, \tag{17}$$

where we have dropped the overall position independent factors multiplying the expressions, and replaced z and κ with their earlier definitions. These two asymptotic solutions are clearly combinations of plane waves $\exp(\pm ikx)$ multiplied by exponentials with logarithmic exponents, which for real A/k represent logarithmic corrections to the phase of the wave, and for imaginary A/k an overall growth or diminishing of the wave. The logarithmic terms cannot be neglected at large $|x|$ and are present due to the slow decay of the profile as $|x| \to \infty$.

As the waves given in (15) and (16) are not of the form $\exp(\pm ikx)$ at infinity, one might question whether our above identification of "left-going" and "right-going" waves from the contours C_1 and C_2 in Fig. 1 was reasonable. One indication that our intuition is correct can be found in a WKB analysis of the Helmholtz equation we started with (4) (see, e.g., [19]) where the two solutions representing the propagation of left- and right-going waves in the absence of reflection and are, for large $|x|$,

$$\begin{aligned} E_{z,\mathrm{WKB}\pm} &= \left(k^2 - \frac{Ak_0^2}{x+ix_0}\right)^{-1/4} \\ &\quad \times \exp\left(\pm i \int_0^x \sqrt{k^2 - \frac{Ak_0^2}{x'+ix_0}}\, dx'\right) \\ &\sim \frac{1}{\sqrt{k}} \exp\left(\pm ikx \mp \frac{iAk_0^2}{2k}\log(1 - ix/x_0)\right), \end{aligned} \tag{18}$$

in agreement with what we identified as left- and right-going waves in (15) and (16). Indeed, in WKB analyses of wave propagation in inhomogeneous media it is common to define the reflectivity and transmissivity for *real* permittivity profiles that do not decay slowly to unity, sometimes even diverging at infinity (such as the linear and quadratic profiles treated in [19]). To calculate, e.g., reflectivity in such cases one takes the relative magnitude of the two WKB waves $|E_{z,\mathrm{WKB}-}/E_{z,\mathrm{WKB}+}|$ on the left of the profile (assuming there is no incoming left-going wave on the right). For real valued profiles where $\epsilon'/\epsilon \to 0$ at infinity, this value for the reflectivity is unambiguous and approaches a constant as $|x| \to \infty$.

In addition in our case all other x dependent factors in (15) and (16) are typically slowly varying compared to $e^{\pm ikx}$, so that the component waves are very close in form to right- and left-going plane waves. This intuition will be further substantiated in the next section where we consider the corresponding Poynting vector. Moreover, in the case $\mathrm{Im}[A] = 0$ the reflectivity and transmissivity can be calculated straightforwardly, given that the *amplitudes* of the left- and right-going parts of (15) and (16) at infinity are asymptotically constant. We obtain

$$\begin{aligned} T_L &= T_R = e^{-\frac{\pi k_0^2 A}{k}}, \quad R_L = 0, \\ R_R &= \left|\frac{2\pi e^{-2kx_0} e^{-\frac{\pi k_0^2 A}{2k}}}{\Gamma\left(1-\frac{ik_0^2 A}{2k}\right)\Gamma\left(-\frac{ik_0^2 A}{2k}\right)}\right|^2 \\ &= 4e^{-4kx_0} e^{-\frac{\pi k_0^2 A}{k}} \sinh^2\left(\frac{\pi k_0^2 A}{2k}\right), \end{aligned} \tag{19}$$

where the subscripts "L" and "R" indicate the cases of incidence from the left and right of the profile, respectively. We can see that the profile (2) does not reflect waves incident from the left, independent of the values of A (real), $k > 0$ and $x_0 > 0$. This is in accordance with our discussion of the behavior of the two contours C_1 and C_2 shown in Fig. 1 as well as with the findings presented in [9]. For real values of A/k there is always some reflection for incidence from the right, although this can become exponentially small for large values of kx_0, when the profile varies very slowly compared to the wavelength. In the opposite limit $kx_0 \ll 1$ and $k_0 A \gg 1$ the reflection and transmission coefficients (19) reduce to $T_L = T_R = R_L = 0$ and $R_R = 1$ so that the profile acts as a perfect reflector for waves incident from the right, and a perfect absorber for waves incident from the left, properties which in the ideal case hold for all angles of incidence. Although we derived the above reflectivity R_R for $\mathrm{Im}[A] = 0$, note that it vanishes for the purely imaginary values of A where $A = -2kmi/k_0^2$ ($m \geqslant 0$, integer), where the argument of one or both of the gamma functions is a negative integer or zero. For these values of A the profile is PT symmetric and for a large fixed $|x|$ the transmitted wave has the same amplitude as the incident one, with a phase difference that is a multiple of π, bearing quite a close similarity with the behavior of PT-symmetric media at the symmetry breaking point [20].

When $\mathrm{Im}[A] \neq 0$ the amplitude of the exact solution [(15) and (16)] is not asymptotically constant, and it is not straightforward to analyze the reflectivity and transmissivity of the profile. For $k_0 A = +i$, for instance, the amplitude of the incident left-going wave in (16) approaching $x = 0$ from $+\infty$ is amplified, as is the reflected right-going wave moving towards $+\infty$, while the amplitude of the transmitted left-going wave moving towards $-\infty$ is damped. This behavior occurs due to the scattering profile (2) being lossy for $x < 0$ while exhibiting gain for $x > 0$, even in the limit $|x| \to \infty$. Yet, even in this case $\mathrm{Im}[A] \neq 0$, it is possible to assess the *reflectionless* behavior of the profile given in (2), which is analytic in the upper half position plane and therefore ought to be nonreflecting for waves incident from the left [9]. Although we cannot unambiguously define a reflection coefficient for

the profile in these cases, one way to ascertain when the reflectivity is zero is to consider the Poynting vector $\boldsymbol{S} = \boldsymbol{E} \times \boldsymbol{H}$ corresponding to the solution calculated above.

III. THE POYNTING VECTOR

The problem of determining the reflectivity of the profile (2) when $\mathrm{Im}[A] \neq 0$ is similar to finding the reflectivity of waves incident onto the interface between two homogeneous media where the refractive indices are complex. In such cases the amplitudes of the waves also do not tend to constant values at infinity, but exponentially increase or decrease depending on the direction of propagation and whether the material exhibits loss or gain. We initially consider the case [1] of a uniform (nonmagnetic and isotropic) medium having a complex index of refraction $n = n_R + in_I = \sqrt{\epsilon}$ in which two monochromatic counterpropagating waves are given by

$$\begin{aligned} \boldsymbol{E}_{\pm}(x,t) &= \alpha_{\pm} e^{\pm i n_R k_0 x} e^{\mp n_I k_0 x} e^{-e\omega t}\hat{\boldsymbol{z}} \equiv \alpha_{\pm}\mathcal{E}_{\pm}(x) e^{-i\omega t}\hat{\boldsymbol{z}}, \\ \boldsymbol{B}_{\pm}(x,t) &= \frac{i}{\omega}\alpha_{\pm}\frac{\partial \mathcal{E}_{\pm}(x)}{\partial x} e^{-i\omega t}\hat{\boldsymbol{y}}. \end{aligned} \tag{20}$$

The time-averaged Poynting vector $\langle \boldsymbol{S}\rangle = \langle \boldsymbol{E} \times \boldsymbol{H}\rangle$ (note in our case $\mu = 1$ so that $\boldsymbol{B}$ and $\boldsymbol{H}$ differ only by factor of μ_0) in the presence of both counterpropagating waves $\boldsymbol{E} = \boldsymbol{E}_+ + \boldsymbol{E}_-$ is

$$\begin{aligned} \langle \boldsymbol{S}(x)\rangle \;=\; & \frac{1}{2\mu_0 c}\{n_R(|\alpha_+|^2 e^{-2n_I k_0 x} - |\alpha_-|^2 e^{2n_I k_0 x}) \\ & + 2n_I \mathrm{Im}[\alpha_-\alpha_+^{\star} e^{-2in_R k_0 x}]\}\hat{\boldsymbol{x}}, \\ \to\; & \frac{1}{2\mu_0 c}[n_R\,(|r|^2 e^{-2n_I k_0 z} - e^{2n_I k_0 z}) \\ & - 2n_I |r|\sin(2n_R k_0 x + \phi)]\hat{\boldsymbol{x}}, \end{aligned} \tag{21}$$

where we applied the general result $\langle \mathrm{Re}[ae^{-i\omega t}]\mathrm{Re}[be^{-i\omega t}]\rangle = (1/2)\mathrm{Re}[ab^{\star}]$ and in the last line have set $\alpha_- \to 1$ and $\alpha_+ \to r = |r|\exp(i\phi)$, considering the left-going wave as "incident" and the right-going one as "reflected." When $n_I = 0$ the Poynting vector is independent of position and is simply the sum of the two energy fluxes corresponding to the presence of only one wave at a time (the right-going one contributing positively, and the left-going one negatively). Meanwhile for $n_I \neq 0$, the individual contributions to the flux from the left- and right-going waves depend exponentially on position. Moreover, the net energy flux is not simply the sum of these two contributions, but includes an additional rapidly varying "interference" contribution which oscillates with an amplitude independent of position. This spatially oscillating term simply conveys extra energy to the regions where it is dissipated most (for $n_I > 0$) or away from the regions where it is amplified most (for $n_I < 0$), i.e., where the amplitude of the electric field is larger due to the constructive interference of the two counterpropagating waves. This spatially oscillating contribution to the total energy flux is a qualitative hallmark of the presence of two counterpropagating waves in a medium with gain or loss.

We now examine the Poynting vector of the exact solution for propagation in the profile (2) given by (15) for $x \to -\infty$, i.e., the side onto which the waves are incident, and consider for the sake of comparison with (21) the case of normal incidence: $k = k_0 = \omega/c$. As above we obtain the corresponding magnetic field ($\boldsymbol{B} = \mu_0 \boldsymbol{H}$) from the Maxwell equation $\nabla \times \boldsymbol{E} = i\omega \boldsymbol{B}$:

$$\boldsymbol{B}_1 = B_{y1}(x)\, e^{-i\omega t}\,\hat{\boldsymbol{y}} = -\frac{1}{c}\left(1 - \frac{A}{2x}\right) E_{z1}(x)\, e^{-i\omega t}\,\hat{\boldsymbol{y}}. \tag{22}$$

Note that for large $|x|$ we have $1 - A/(2x) \simeq n_R(x) + in_I(x) \equiv \sqrt{\epsilon(x)}$. The time-averaged Poynting vector is then

$$\begin{aligned} \langle \boldsymbol{S}_1(x)\rangle &= -\frac{1}{2\mu_0}\,\mathrm{Re}[E_{z1}^{*}(x)\, B_{y1}(x)]\hat{\boldsymbol{x}}, \\ &= \frac{1}{2\mu_0 c}\left(1 - \frac{\mathrm{Re}[A]}{2x}\right)|E_{z1}(x)|^2\hat{\boldsymbol{x}} \\ &\approx \frac{n_R(x)}{2\mu_0 c} e^{k_0 \mathrm{Im}[A]\log(2k_0|x|)}\hat{\boldsymbol{x}}, \end{aligned} \tag{23}$$

which depends on position, but does not exhibit any spatially rapidly oscillating contribution and is directly analogous to (21) (for incidence from the opposite direction) with $r = 0$.

For waves incident from the opposite side of the profile (2) the Poynting vector is computed from (16) for $x \to +\infty$. The magnetic field is now given by

$$\begin{aligned} \boldsymbol{B}_2 &= B_{y2}(x) e^{-i\omega t}\,\hat{\boldsymbol{y}} \\ &= \frac{1}{c}(n_R(x) + in_I(x))\Big[e^{-ik_0 x + \frac{iAk_0}{2}\log(2k_0|x|)} \\ &\quad - re^{ik_0 x - \frac{iAk_0}{2}\log(2k_0|x|)}\Big]\hat{\boldsymbol{y}}, \end{aligned} \tag{24}$$

where r is now given by (17). The time-averaged Poynting vector is

$$\begin{aligned} \langle \boldsymbol{S}_2(x)\rangle &= -\frac{1}{2\mu_0}\mathrm{Re}[E_{z2}^{\star}(x)\, B_{y2}(x)]\hat{\boldsymbol{x}} \\ &= -\frac{1}{2\mu_0 c}[n_R(x)(e^{-\mathrm{Im}[A]k_0\log(2k_0|x|)} \\ &\quad - |r|^2 e^{\mathrm{Im}[A]k_0\log(2k_0|x|)}) \\ &\quad + 2|r|n_I(x)\sin(2k_0 x - k_0\mathrm{Re}[A]\log \\ &\quad \times (2k_0|x|) + \phi)]\hat{\boldsymbol{x}}, \end{aligned} \tag{25}$$

which exhibits rapid spatial oscillations and has the same form of Eq. (21), albeit with a power law decay or growth rather than an exponentially varying one.

As shown by the asymptotic solutions of the Helmholtz Eq. (4) [(15 and 16)], when $\mathrm{Im}[A] \neq 0$ the amplitudes of the waves do not reach a constant value at $x \to \pm\infty$ and thus the reflectivities $R_{R,L}$ and transmissivity T cannot be defined in the usual way as asymptotic intensity ratios [as done in (19) for $\mathrm{Im}[A] = 0$]. As mentioned above, this is simply due to the fact that gain and loss decay too slowly to zero and they are not asymptotically negligible. This situation is closely related to the one occurring within a homogeneous medium with a complex refractive index [as described by (21)] in which case it is also impossible to define the reflectivity in the standard way due to the exponentially growing or decaying factors. However, the presence or absence of two counterpropagating waves can be assessed via the presence or absence of rapid spatial oscillations in the energy flux. Therefore, we conclude from the qualitative behavior of the Poynting vector (23) that this represents a right-going wave which is *not* reflected,

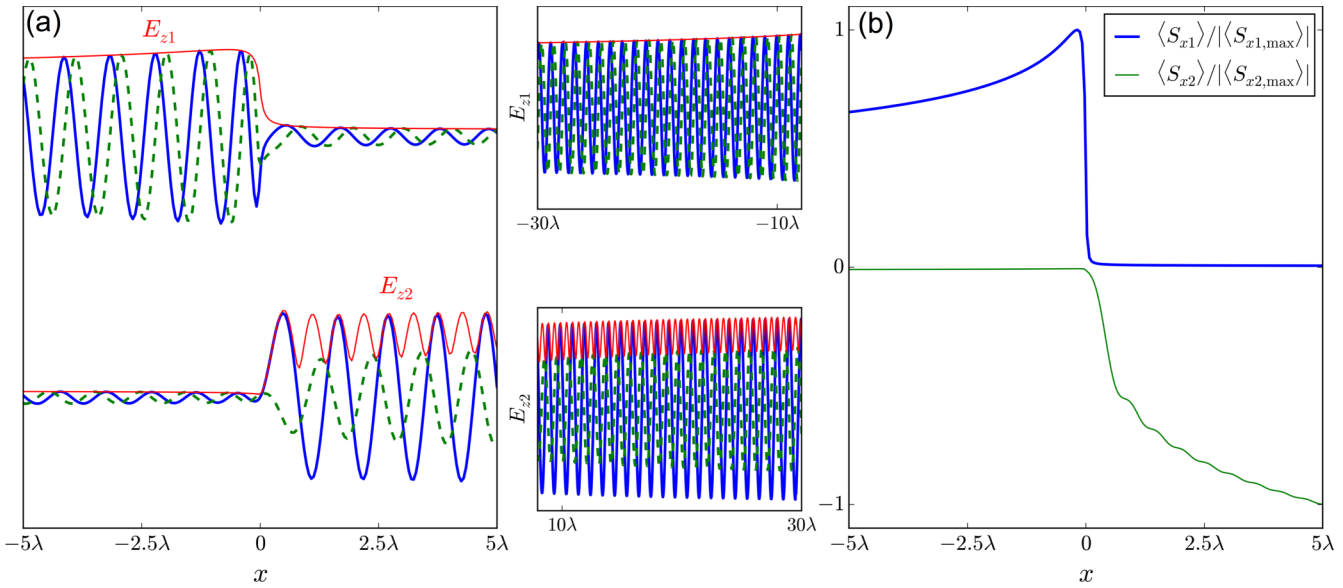

FIG. 2. (a) Shows the two exact solutions E_{z1} and E_{z2} of the Helmholtz Eq. (4) in the permittivity profile (2), numerically computed from (5) and the contour integral representation (7) with the two contours shown in Fig. 1 (the two plots are offset vertically for the purposes of visualization, and the units on the x axis are $\lambda = 2\pi/k_0$). These two forms for the electric field correspond to waves incident from the left and right of the profile, respectively. The choices of parameters defining the profile are $k_0 A = 1.5 - 0.2i$ and $k_0 x_0 = 0.15$, and the waves are at normal incidence $k_y = 0$. Blue solid and green dashed lines are the real and imaginary parts of $E_z(x)$ and the thinner red line is the absolute value. This particular profile is an example where the wave amplitude is not asymptotically constant, and the two smaller middle panels show the behavior of the waves over a larger scale where a slow change in the overall wave amplitude is evident. (b) Shows the normalized Poynting vector $\langle S_x\rangle(x)/|\langle S_{x,\max}\rangle|$ calculated from $\langle S_x\rangle = -(1/(2\mu_0))\mathrm{Re}[E_z^\star B_y]$, normalized such that the maximum value in the plot is ± 1. The upper blue line is calculated for the wave incident from the left (E_{z1}), whereas the lower thinner green line is for the wave incident from the right (E_{z2}). The lack of any rapid oscillations in the former case indicates a lack of reflection [c.f. Eq. (23)], whereas the rapid oscillations in the latter indicates reflection [c.f. Eq. (25)].

whereas (25) corresponds to the superposition of a left-going incident wave and a right-going reflected wave. The exact solutions shown in Fig. 2 both at small and large distances thus exhibit the reflectionless or reflective behavior outlined in Sec. I and are in accordance with the results of [9].

IV. PULSE PROPAGATION

While the exact solutions of the Helmholtz equation considered above allow for a detailed analysis of the asymptotic behavior of monochromatic waves incident onto the permittivity profile (2) from the left or from the right, the physical meaning of reflection (or lack of it) and transmission can be further illustrated considering the propagation of finite wave packets. This also models the more experimentally feasible where the reflectivity of the profile is assessed without considering propagation through the whole (infinite) structure. We note that although it is impossible to have the complex spatial distribution of material properties (2) for all the component frequencies in an arbitrary pulse (due to the *frequency domain* Kramers-Kronig relations), we imagine some bandwidth over which (2) is valid. Here we discuss several numerically calculated examples of pulse propagation for the same profile as in Fig. 2, for normal incidence $k = k_0$. The pulse propagation is found through solving the Helmholtz equation in the presence of a source at $x = x_0$,

$$\left[\frac{d^2}{dx^2} + k_0^2\epsilon(x)\right] E_z(x,\omega) = -i\omega\mu_0 \mathcal{J}_z(\omega)\delta(x - x_0),$$

which has the exact solution,

$$E_z(x,\omega) = -i\mu_0\omega\mathcal{J}_z(\omega)\frac{\Theta(x - x_0)E_{z1}(x)E_{z2}(x_0) + \Theta(x_0 - x)E_{z1}(x_0)E_{z2}(x)}{E'_{z1}(x_0)E_{z2}(x_0) - E_{z1}(x_0)E'_{z2}(x_0)}, \tag{26}$$

with E_{z1} and E_{z2} given by the integral representations in Sec. I. Assuming a Gaussian spectrum $\mathcal{J}_z(\omega) = \mathcal{J}_0 \exp(-(\omega - \Omega_0)^2/(\Delta\omega)^2)$, where Ω_0 is the central frequency of the pulse, $\Delta\omega$ is the bandwidth, and $\mathcal{J}_0$ sets the overall amplitude, the time-dependent field $E_z(x,t)$ is calculated as an integral over (26) for different frequencies ω,

$$E_z(x,t) = \int_{-\infty}^{\infty} E_z(x,\omega)e^{-i\omega t}\frac{d\omega}{2\pi}.$$

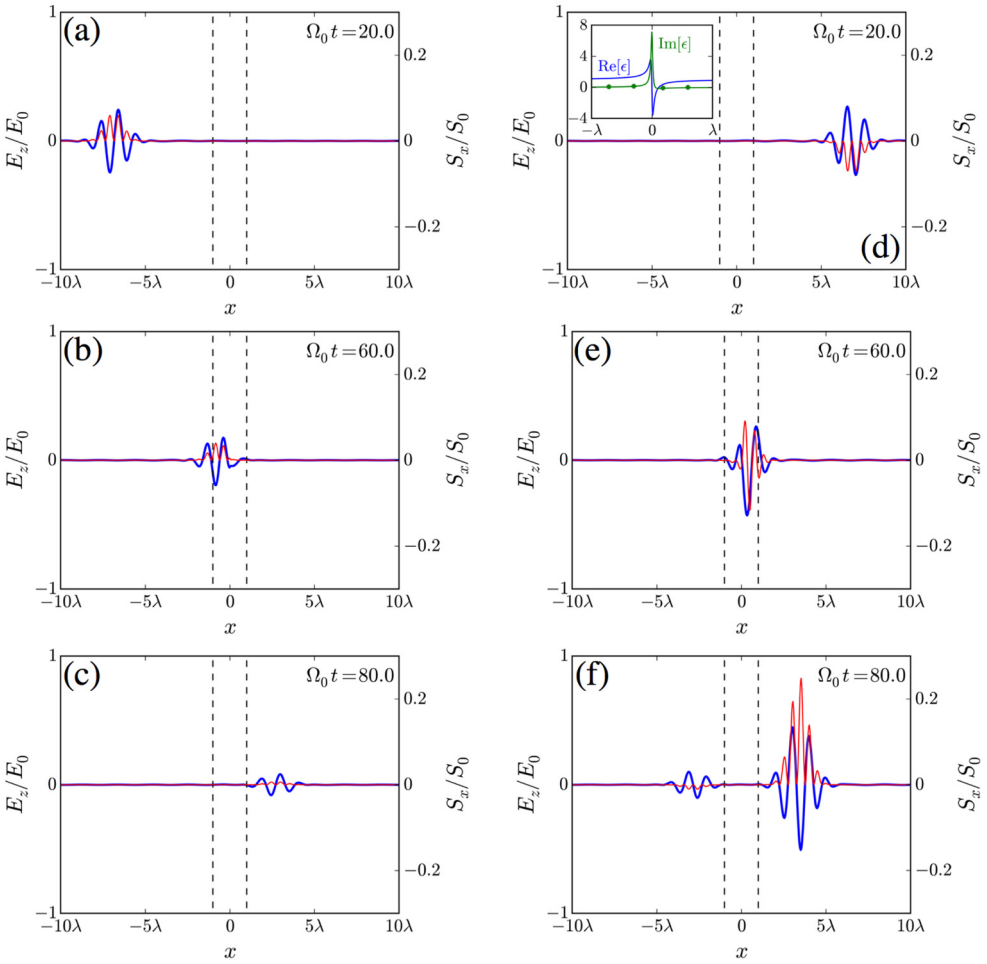

FIG. 3. A Gaussian pulse is launched with central frequency $\Omega_0 = cK_0 = 2\pi c/\lambda$ generated by a current localized at positions $x = -10\lambda$ (a)–(c), and $x = 10\lambda$ (d)–(f) with a bandwidth of $\Delta\Omega = 0.3\,\Omega_0$. The electric field (thicker blue line) and Poynting vector (thinner red line) are given in units of $E_0 = \mu_0 c \mathcal{J}_0 \Omega_0$ and $S_0 = E_0^2/(\mu_0 c)$, respectively. The vertical dashed lines indicate the region over which the permittivity is plotted in the inset of (d) (real part, blue solid and imaginary part green with circles). It is imagined that over this bandwidth the permittivity is given by (2) for the parameters $K_0 A = 0.7 + 0.2i$ and $K_0 x_0 = 0.1$ (a profile that contains regions of gain). It is useful to list these parameters for a realistic case. For example, for a central frequency in the microwave regime $\Omega_0 = 10^{10}\,\mathrm{rad\,s^{-1}}$ we have $\lambda = 0.18\,\mathrm{m}$, $\Delta\Omega = 3 \times 10^9\,\mathrm{rad\,s^{-1}}$, $A/x_0 = 7 + 2i$ and $x_0 = 0.003\,\mathrm{m}$, which illustrates that these large index variations on the scale of millimeters will not reflect centimeter scale waves. Notice that the reflectionless behavior is clearly identified: (a)–(c) For a source on the left there is no reflected pulse, while (d)–(f) for a source on the right there is.

Our results are summarized in Figs. 3–5, showing that the reflection is essentially confined to the central region of the profile, and that from one side the pulse passes through the central region without generating a reflected pulse. From the asymptotic form of the waves in the profile [(15) and (16)], we observe that for real A the transmitted pulse is reshaped, with an exponential reduction of the higher frequency components by the factor $\exp(-\pi A k_0/2)$. For purely imaginary A the frequency components undergo a phase shift, equivalent to a displacement of the pulse by a distance $\pi|A|/2$. The inset of Fig. 3(d) shows the permittivity profile through which the pulse propagates. For incidence from the left the pulse passes through a region of increasing real and imaginary ϵ, before the real part suddenly drops to a negative value and then returns to the background. Approached in this order, this does not generate a reflected pulse. Meanwhile for incidence from the right the pulse starts in the background region before encountering a sudden drop in the real part of the permittivity to a negative value (where there is also some degree of material gain), which generates a significant reflection.

V. TRUNCATING AN INFINITE PROFILE

Even if they asymptotically tend to a constant background value, the reflectionless permittivity profiles obeying the spatial Kramers-Kronig relations [9] are always, strictly speaking, of infinite extent, while a realistic sample will correspond in practice to a suitable truncation of such a profile. In this section, we discuss the effect of introducing such a truncation, and finally we show how multiplying the reflectionless potential with a very rapidly decaying and smooth function will preserve the reflectionless behavior apart from the case of grazing incidence [9].

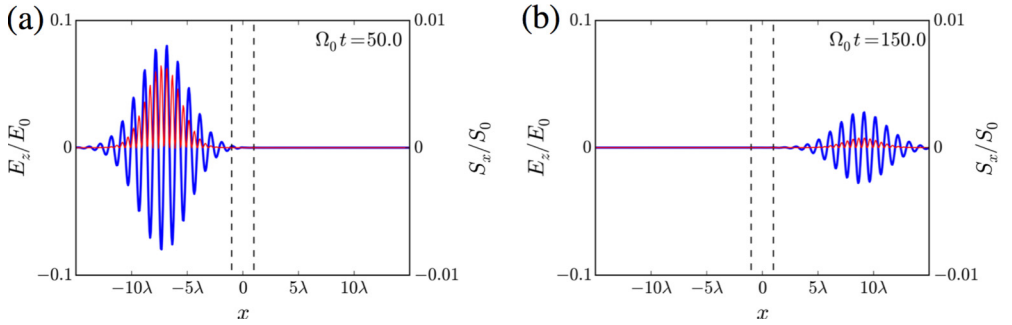

FIG. 4. As in Fig. 3, but for a narrower pulse bandwidth of $\Delta\Omega = 0.1\,\Omega_0$, demonstrating that the nonreflecting behavior from the left is not dependent on the pulse width.

The simplest kind of truncation is to terminate the profile (2) at some distance from the origin $|x| = L/2$, and set $\epsilon = 1$ for $|x| > L/2$. However, in general such a truncation leads to significant reflection due to the steplike discontinuity in $\epsilon(x)$, and this reflection increases markedly as the angle of incidence is increased towards $\pi/2$. The next simplest truncation is to retain the continuity of $\epsilon(x)$, setting the permittivity to its final value $\epsilon = \epsilon_{\mathrm{R,L}} = \epsilon(\pm L/2)$ for $|x| > L/2$. We can calculate the effect of such a truncation exactly, constructing the transfer matrix [21] for propagation between the two homogeneous regions where $\epsilon = \epsilon_{\mathrm{R,L}}$. We write the field in the three different regions as

$$E_z(x) = \begin{cases} \alpha_{\mathrm{L}}^{(+)} e_{\mathrm{L}}^{(+)}(x) + \alpha_{\mathrm{L}}^{(-)} e_{\mathrm{L}}^{(-)}(x) & x < -L/2 \\ A_1 E_{z1}(x) + A_2 E_{z2}(x) & -L/2 < x < L/2, \\ \alpha_{\mathrm{R}}^{(+)} e_{\mathrm{R}}^{(+)}(x) + \alpha_{\mathrm{R}}^{(-)} e_{\mathrm{R}}^{(-)}(x) & x > L/2 \end{cases} \tag{27}$$

where $e_{\mathrm{L}}^{(\pm)} = \exp[\pm i k_{\mathrm{L}}(x + L/2)]$ and $e_{\mathrm{R}}^{(\pm)} = \exp[\pm i k_{\mathrm{R}}(x - L/2)]$ with $k_{\mathrm{R,L}} = \sqrt{\epsilon_{\mathrm{R,L}} k_0^2 - k_y^2}$. Demanding the continuity of $E_z(x)$ and $E_z'(x)$ across the three regions (27) leads to the pair of matrix equations,

$$\begin{pmatrix} 1 & 1 \\ ik_{\mathrm{L}} & -ik_{\mathrm{L}} \end{pmatrix} \begin{pmatrix} \alpha_{\mathrm{L}}^{(+)} \\ \alpha_{\mathrm{L}}^{(-)} \end{pmatrix} = \begin{pmatrix} E_{z1}(-L/2) & E_{z2}(-L/2) \\ E_{z1}'(-L/2) & E_{z2}'(-L/2) \end{pmatrix} \begin{pmatrix} A_1 \\ A_2 \end{pmatrix},$$

and

$$\begin{pmatrix} E_{z1}(L/2) & E_{z2}(L/2) \\ E_{z1}'(L/2) & E_{z2}'(L/2) \end{pmatrix} \begin{pmatrix} A_1 \\ A_2 \end{pmatrix} = \begin{pmatrix} 1 & 1 \\ ik_{\mathrm{R}} & -ik_{\mathrm{R}} \end{pmatrix} \begin{pmatrix} \alpha_{\mathrm{R}}^{(+)} \\ \alpha_{\mathrm{R}}^{(-)} \end{pmatrix},$$

which can be combined to eliminate A_1 and A_2, thus obtaining the transfer matrix for propagation across the truncated profile,

$$\begin{aligned} &\begin{pmatrix} \alpha_{\mathrm{R}}^{(+)} \\ \alpha_{\mathrm{R}}^{(-)} \end{pmatrix} \\ &= \frac{i}{2k_{\mathrm{R}}} \frac{1}{E_{z1}(-L/2)E_{z2}'(-L/2) - E_{z2}(-L/2)E_{z1}'(-L/2)} \\ &\quad \times \begin{pmatrix} b_{1+}a_{1-} - b_{2+}a_{2-} & b_{2+}a_{1+} - b_{1+}a_{2+} \\ b_{1-}a_{2-} - a_{1-}b_{2-} & b_{1-}a_{2+} - b_{2-}a_{1+} \end{pmatrix} \begin{pmatrix} \alpha_{\mathrm{L}}^{(+)} \\ \alpha_{\mathrm{L}}^{(-)} \end{pmatrix}, \end{aligned} \tag{28}$$

where

$$\begin{aligned} a_{n\pm} &= E_{zn}'(-L/2) \pm i k_{\mathrm{L}} E_{zn}(-L/2), \\ b_{n\pm} &= E_{zn}'(L/2) \pm i k_{\mathrm{R}} E_{zn}(L/2). \end{aligned} \tag{29}$$

From an examination of (28) it is clear that if there is no wave incident from the right $\alpha_{\mathrm{R}}^{(-)} = 0$ then the ratio of left- and right-going waves on the left of the profile is given by

$$\frac{\alpha_{\mathrm{L}}^{(-)}}{\alpha_{\mathrm{L}}^{(+)}} = -\frac{b_{1-}a_{2-} - b_{2-}a_{1-}}{b_{1-}a_{2+} - b_{2-}a_{1+}}, \tag{30}$$

when (30) vanishes then the truncated profile can be said to be reflectionless from the left. An examination of the asymptotic form of the solution E_{z1} (15) shows that on both the left and the right of the profile we have $E_{z1}' - ik_{\mathrm{L,R}}E_{z1} = 0$ and thus $b_{1-} = a_{1-} = 0$ implying that (30) is zero. Therefore, so long as the asymptotic limit (15) is valid (which requires terms of order $1/x^2$ to be vanishingly small in comparison to $1/x$) then truncation of the profile to a constant value at $\pm L/2$

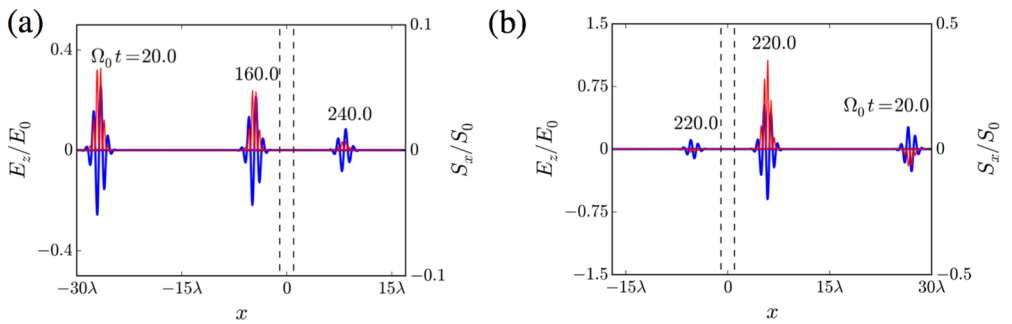

FIG. 5. As in Fig. 3, but for sources located at $x = -30\lambda$ (a) and $x = +30\lambda$ (b). The slow decay to zero of the imaginary part of $\epsilon(x)$ causes the amplitude of the pulse to slowly grow or diminish as it propagates towards the central region of the profile (numbers within the plots indicate different times), but the qualitative character of the nonreflecting behavior from the left is not affected.

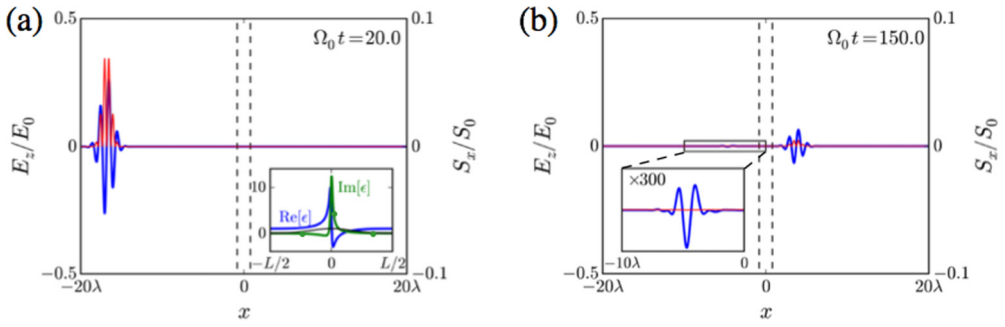

FIG. 6. A pulse is launched at $x = -20\lambda$ (a) and propagates through the permittivity profile (31) (real part blue solid, imaginary part green with circles), for the values $K_0 A = 1.2 - 0.5i$, $K_0 x_0 = 0.1$, $L = 1.6\lambda$, and $\Delta x = 0.39\lambda$, truncated to a value of 1 at the vertical dashed lines. The inset of (a) shows the permittivity profile within the dashed lines, along with the Gaussian envelope function (black solid line). (b) Shows the pulse shape after propagation through the truncated profile, with only very slight reflection evident (inset plot is a 300 times magnification of the reflected pulse, plotted with the same vertical range as the main panel).

does not introduce any reflection. However, the validity of the asymptotic limit requires $kx \gg 1$, which requires an ever larger value of L as the wave approaches grazing incidence.

The reflection can be further reduced if the profile (2) is multiplied by an envelope function before it is truncated so that $\epsilon(x)$ and all its derivatives are close to continuous at $x = \pm L/2$. Figure 6 shows pulse propagation through a profile multiplied by a Gaussian envelope before truncation:

$$\epsilon(x) = \begin{cases} 1 - \frac{A}{x + i x_0} e^{-\frac{x^2}{\Delta x^2}} & |x| \leqslant L/2 \\ 1 & |x| > L/2 \end{cases}. \tag{31}$$

As shown in Fig. 6, smoothly truncating the potentials has very little effect on the reflectionless behavior. As a matter of fact, the truncation method above [9] is quite distinct from a sharp boxlike truncation, such as that used, for instance, in [22,23], because the slowly varying envelope function avoids the large discontinuities that may occur at abrupt interfaces which can lead to significant reflection even at normal incidence due to constructive interference between reflections at the entrance and exit faces of the sample.

VI. CONCLUSIONS

When considering propagation through the profile (2), it is impossible to unambiguously define the reflection and transmission coefficients for waves incident from the left or right if $\mathrm{Im}[A] \neq 0$. This is a particular case of the condition (1) discussed by Longhi [11], and bears much similarity with the problem of defining reflection and transmission coefficients between two homogenous media with complex refractive indices. Nevertheless, just as in that simpler case it *is* possible to say when there is *zero* reflection.

In this work we discussed a particular medium satisfying the spatial Kramers-Kronig relations where there is an exact solution to the Helmholtz equation that can be represented as a contour integral. The two component waves can be identified as the two points of the stationary phase of the integrand (9) that approach the two branch points of (8) as $|x| \to \infty$. For incidence from one side, only one of these two points ever contributes to the integral, whereas for incidence from the other side, both points contribute. We thus conclude that even when (1) is not satisfied, the profile is still reflectionless from one side even though we cannot unambiguously say what the reflection coefficient is for incidence from the other side. This result was bolstered through considering (i) the form of the Poynting vector which exhibits rapid oscillations in the dissipative region of the profile when there is reflection, and (ii) the propagation of a wave packet launched from a source embedded within the profile, which we illustrated in Figs. 3–5, demonstrating that reflected pulses are only generated when the source is placed on the right-hand side of the profile (2). The ambiguity in the scattering from (2) disappears when the profile is truncated to a finite width L and we have demonstrated that this truncation can be achieved while largely retaining the reflectionless behavior.

ACKNOWLEDGMENTS

S.A.R.H. wishes to thank S. Longhi, T. G. Philbin, and C. G. King for useful conversations, and the EPSRC for financial support under program Grant No. EP/I034548/1. S.A.R.H. also acknowledges financial support from the Royal Society and TATA.

[1] J. D. Jackson, *Classical Electrodynamics* (John Wiley, New York, 1999).
[2] M. V. Berry, J. Phys. A **15**, 3693 (1982).
[3] J. B. Pendry, D. Schurig, and D. R. Smith, Science **312**, 1780 (2006).
[4] G. Pöschl and E. Teller, Z. Phys. **83**, 143 (1933).
[5] M. V. Berry and C. J. Howls, J. Phys. A **23**, L243 (1990).
[6] J. Lekner, Am. J. Phys. **875**, 1151 (2007).
[7] S. A. R. Horsley, J. Opt. **18**, 085104 (2016).

[8] I. M. Gelfand and B. M. Levitan, Am. Math. Soc. Trans. **1**, 253 (1955).
[9] S. A. R. Horsley, M. Artoni, and G. C. La rocca, Nature Photonics **9**, 436 (2015).
[10] S. A. R. Horsley, C. G. King, and T. G. Philbin, J. Opt. **18**, 044016 (2016).
[11] S. Longhi, Eur. Phys. Lett. **112**, 64001 (2015).
[12] L. D. Landau and E. M. Lifshitz, *Electrodynamics of Continuous Media* (Pergamon Press, Oxford, 1960).
[13] M. V. Berry, J. Phys. A **31**, 3493 (1998).
[14] G. W. Milton, Physica B **338**, 186 (2003).
[15] Z. Ahmed, C. M. Bender, and M. V. Berry, J. Phys. A **38**, L627 (2005).
[16] T. G. Philbin, J. Opt. **18**, 01LT01 (2016).
[17] NIST Digital Library of Mathematical Functions, http://dlmf.nist.gov/, Release 1.0.10 of 2015-08-07.
[18] I. S. Gradshteyn and I. M. Ryzhik, *Table of Integrals, Series and Products* (Elsevier, Amsterdam, 2007).
[19] J. Heading, *An Introduction to Phase-Integral Methods* (Dover, Mineola, 2013).
[20] Z. Lin, H. Ramezani, T. Eichelkraut, T. Kottos, H. Cao, and D. N. Christodoulides, Phys. Rev. Lett. **106**, 213901 (2011).
[21] M. Born and E. Wolf, *Principles of Optics* (Pergamon, Oxford, 1964).
[22] S. Longhi, J. Phys. A **44**, 485302 (2011).
[23] A. Mostafazadeh, Phys. Rev. A **89**, 012709 (2014).